Sustainable Energy & Fuels

ROYAL SOCIETY OF CHEMISTRY

PAPER

View Article Online
View Journal | View Issue

Cite this: *Sustainable Energy Fuels*, 2026, **10**, 2548

An integrated techno-economic-environmental-policy assessment of supercritical biodiesel production: pathway to competitiveness

Jon Selimi, †[ab] Abdullah H. Albin Saad,†[c] Essra R. Altahir,[d] Mayasem A. Alsuhami,[c] Mohd A. Khan, *[ce] Rashed M. Aleisa,*[c] Christian P. Hulteberg[ab] and Omar Y. Abdelaziz *[df]

Despite its promise, biodiesel production *via* the supercritical methanol (SCM) process has stalled due to limited understanding of interactions among key operating parameters and process-modeling gaps, resulting in contradictory techno-economic (TEA) and life-cycle carbon footprint assessments. In the present study, we integrate experimental optimization with techno-economic, carbon footprint, and policy analyses to identify the path to economic competitiveness for SCM biodiesel production from waste cooking oil (WCO). Response surface modeling based on experimental data was used to quantify interactions among operating parameters and develop a predictive yield model. Under optimal conditions (282.8 °C, 125 bar, methanol-to-oil ratio of 39.17, and reaction time of 43.3 min), biodiesel yield exceeded 92%, and a detailed process flowsheet was developed in Aspen Plus® to quantify material and energy requirements. TEA results indicate that under optimized conditions, SCM biodiesel remains economically challenged, with levelized production costs of 0.9–1.4 $ per kg-biodiesel, depending on plant scale. These costs are driven primarily by high WCO consumption (0.99 kg kg^{-1}-biodiesel) and high-pressure steam demand (3 kg kg^{-1}-biodiesel), required for stoichiometric conversion and energy-intensive distillation, respectively. In contrast, life cycle carbon footprint analysis demonstrates a strong environmental advantage: under renewable electricity and heat supply, SCM biodiesel achieves a carbon intensity of ~0.28–0.30 $kgCO_{2eq}$ per kg-biodiesel, substantially lower than fossil diesel (~4 $kgCO_{2eq}$ per kg-diesel). Finally, yet most importantly, by quantitatively linking process performance, economics, emissions, and policy, this study identifies carbon pricing (~100 $ per t-CO_2) and scale-up as critical levers to reconcile the environmental benefits of SCM biodiesel with commercially viable deployment.

Received 24th December 2025
Accepted 17th April 2026

DOI: 10.1039/d5se01694k

rsc.li/sustainable-energy

1. Introduction

Biodiesel is a sustainable fuel that reduces greenhouse gas emissions (GHG) by recycling the carbon already present in the biosphere. Derived from biogenic carbon sources, such as waste cooking oil (WCO), biodiesel offers significant advantages due to its compatibility with existing fleet engines and transportation infrastructure.[1–3] Biodiesel is a monoalkyl ester derived from plant or animal oils, typically produced through a transesterification reaction with methanol or ethanol.[4,5] However, when utilizing low-cost feedstocks with high free fatty acid (FFA) content, such as WCO, the traditional base-catalyzed transesterification method is ineffective. This is because alkaline catalysts (*e.g.*, NaOH, KOH) react with FFAs to form soap, resulting in reduced biodiesel yield and hindering separation of fatty acid methyl ester (FAME) and glycerin phases. To overcome this limitation, a two-step process involving acid esterification followed by base transesterification is commonly employed in industry. The acid-catalyzed esterification step converts FFAs to FAME, while the subsequent base transesterification step converts triglycerides to FAME. Nevertheless, the two-step method also poses several challenges, including sensitivity to feedstock quality (notably water and high FFA content), prolonged processing times, catalyst neutralization, catalyst recovery, and water removal.[6]

[a]*Division of Chemical Engineering, Department of Process and Life Science Engineering, Lund University, SE-221 00, Lund, Sweden*
[b]*Hulteberg Chemistry & Engineering AB, SE-212 25, Malmö, Sweden*
[c]*Fuels & Chemicals Division, Research & Development Center, Saudi Aramco, Dhahran, 31311, Saudi Arabia. E-mail: rashed.aleisa@aramco.com*
[d]*Department of Chemical Engineering, King Fahd University of Petroleum & Minerals, Dhahran, 31261, Saudi Arabia. E-mail: omar.abdelaziz@kfupm.edu.sa*
[e]*Department of Chemical and Materials Engineering, University of Alberta, Donadeo Innovation Centre for Engineering, Edmonton, Alberta, T6G 1H9, Canada. E-mail: mohd3@ualberta.ca*
[f]*Interdisciplinary Research Center for Refining & Advanced Chemicals, King Fahd University of Petroleum & Minerals, Dhahran, 31261, Saudi Arabia*
† These authors contributed equally to this work.

Supercritical methanol (SCM) transesterification presents a promising, catalyst-free alternative for biodiesel production, enabling the simultaneous conversion of triglycerides and (FFAs) without feedstock limitations.[7] By operating at elevated temperatures and pressures, this process accelerates reaction kinetics, exhibits tolerance to water and impurities, and simplifies post-reaction separation by eliminating the need for catalyst removal and minimizing soap formation.[8] Nevertheless, the SCM process poses challenges due to its high energy demands and process intensity. To mitigate these drawbacks, careful optimization of operating conditions, including methanol-to-oil (M : O) ratio, process design, as well as techno-economic (TEA) and carbon footprint analyses, are crucial to ensure economic and environmental viability.[9]

Saka and Kusdiana[10] were the first to demonstrate biodiesel synthesis under SCM conditions, achieving a yield of 95% within 2 min at 350 °C, 450 bar, and a M : O molar ratio of 42 : 1. However, they noted that extreme conditions can lead to thermal degradation of FAME, compromising biodiesel quality. Reducing reaction severity is therefore crucial, with temperature being a key factor in determining FAME thermal stability.[7] Odisu *et al.*[11] reported that increasing the temperature beyond the alcohol's supercritical point can lead to lower yield. With a 20 : 1 ethanol-to-oil ratio and a 24 min reaction time, they achieved the highest yield at 240 °C. Qadeer *et al.*[12] provided a critical analysis of supercritical biodiesel synthesis, detailing the influence of process parameters on yield and energy efficiency. They report the need for a higher M : O ratio than the stoichiometric 3 : 1 to improve single-phase homogeneity and drive the equilibrium toward alkyl esters. They also note that at elevated temperatures, increasing pressure to at least the alcohol's critical pressure increases triglyceride solubility, suppresses alcohol vaporization, mitigates thermal side reactions, and thereby improves FAME yield. Additionally, the pressure level set during the process is dependent on the alcohol content in the mixture, according to Nan *et al.*[13] An excess of alcohol can reduce overall yield, underscoring the need to optimize the M : O ratio.[14] Under supercritical conditions, reaction times are reduced because the oil and alcohol form a homogeneous phase,[15] but the necessary duration must still be established for the specific reactant mixture and operating conditions. For instance, He *et al.*[16] reported that methyl ester yield from soybean oil increased with residence time in the 240–280 °C range, whereas an early optimum was observed at shorter residence times in the range of 300–340 °C.

Previous studies on SCM biodiesel production have not fully elucidated how temperature, pressure, methanol to oil ratio and residence time shape the final performance, thereby highlighting a significant research gap. Furthermore, there is a pressing need to develop detailed processes design and simulation frameworks to evaluate economic viability, cost drivers, and bottlenecks of the SCM pathway. Existing TEA studies offer contradictory conclusions on the process's profitability, with some asserting its economic attractiveness with a rapid payback period, while others deem it uncompetitive due to high energy costs. A recent TEA study by Nagapurkar *et al.*[17] on SCM with a propane co-solvent to convert WCO to biodiesel found it to be an economically attractive pathway with a rapid payback period of just two years for a 10 600 t per year plant and a break-even selling price of $2.42 per gallon. This profitability was even more pronounced at a larger scale of 128 000 t per year, where the break-even price fell to $1.31 per gallon. Similarly, Lee *et al.*[18] also report the SCM process to be economically attractive resulting in a net present value of $16.45 million, compared to $1.90 million for the base-catalyzed route. This was attributed to the elimination of catalyst costs and simplification of downstream purification steps. In contrast, a study by Sakdasri *et al.*[19] compared the SCM process with a conventional base-catalyzed process found that a low-molar-ratio SCM process (12 : 1 ratio) was economically viable. However, the conventional SCM process was deemed not profitable due to the large amount of methanol required, a conclusion that echoes an earlier study by Marchetti and coworkers.[20] We found that this divergence is driven by a lack of coherent process modeling and a failure to consistently account for critical variables such as economies of scale, specific energy consumption, and accurate determination of raw material costs. In general, key process steps considered in the SCM process include the high-pressure reactor, flash separation, methanol recovery, and FAME purification units. A key missing gap from most reported SCM processes is a water separation unit which is produced *via* the esterification of FFA in WCO. To ensure sustainable operation, it is particularly important to prevent water accumulation when processing high-FFA feedstocks. Excess water might intensify hydrolysis of fatty acid esters and thereby reduce the yield of biodiesel during esterification as also reported by Kusdiana and Saka.[21] Secondly, we also observed that most studies that report economic viability of the SCM process used very low WCO prices (100–200 $ per t) in their assessment. These values are often derived from restaurant-level rebate figures, but they exclude the costs of transport, aggregation, and pre-treatment/clean-up, and therefore underestimate the true price delivered for WCO.

Like the TEA, life cycle analysis (LCA) studies of supercritical-methanol biodiesel reached mixed conclusions, with some finding it less sustainable than conventional processes and others reporting environmental benefits. Kiwjaroun *et al.*[22] and Lombardi *et al.*[23] have shown that the SCM process for biodiesel production has a significantly higher environmental burden compared to conventional base-catalyzed production. The SCM process results in approximately 38% higher environmental impact due to the large amounts of methanol and steam required, outweighing its benefits of simpler mechanics and higher tolerance for FFAs. Additionally, the SCM process has the highest global warming potential (GWP) impact of 0.68 t_{CO_2eq} per t_{WCO}, primarily due to the high heat requirement for excess methanol recovery, with process steam being the dominant factor. However, the above-mentioned studies are in stark contrast to the results published by Morais *et al.*[24] which concluded that SCM method using propane as co-solvent has the lowest carbon emissions in comparison to alkali catalyzed and acid-catalyzed methods Similarly, Nagapurkar *et al.*[17] confirmed that the same SCM method achieves 17% lower CO_2 emissions than the alkali catalyzed process and 4% lower than petroleum diesel, as a result of not using any kind of catalysts.

The relatively modest 4% advantage over diesel's production emissions, however, highlights that a significant portion of the SC process's greenhouse gas footprint stems from fossil-based inputs, primarily methanol and process energy.

The inconsistency in previous LCA results underscores the need for a more rigorous assessment of the SCM process, with a properly defined functional unit and system boundaries. More importantly, clear theme is that methanol usage and its sourcing are pivotal to the life-cycle impacts. Supercritical routes traditionally require a large excess of methanol (often 20–40 : 1 molar ratios), incurring both direct emissions from producing that methanol (typically from natural gas) and indirect emissions from the energy needed to heat and recover it. If this methanol is derived from fossil sources, it introduces a significant fossil carbon component into an otherwise renewable fuel cycle, and this has not been assessed in previous studies.

To address these research gaps, in this study, we present an integrated assessment of biodiesel production from WCO under non-catalytic SCM conditions. Unlike previous studies that focused on catalyst-enhanced systems, generalized feedstocks, or solely simulation approaches, this work presents a unified framework combining experimental optimization *via* RSM, development of a reduced quadratic regression model for predicting biodiesel yield. The experimental results guide the process design and simulation followed by detailed TEA and carbon footprint analysis, providing a holistic framework for the evaluation of the sustainability of the process. This integrated experimental–modeling approach provides valuable insights for promoting the economic and environmental viability of supercritical biodiesel production and advancing industrial-scale waste-to-energy strategies.

2. Materials and methods

2.1. Materials

The WCO used in this study was waste rapeseed oil collected from a local fast-food restaurant in Malmö, Sweden. Prior to use, it was filtered through a 20 μm filter to remove residual food particles that could interfere with the biodiesel production. Methanol (≥99.9%, anhydrous, Merck) was used as the solvent. Identification of FAME components in the biodiesel samples were carried out using a certified FAME standard solution (C_8–C_{24}, Merck), with methyl heptadecanoate employed as an internal standard (≥99.0%, Merck). Carbon disulfide (CS_2, ≥99.9%, Merck) served as the solvent for gas chromatography (GC) analysis.

2.2. Gas chromatography

The oil samples were analyzed using a GC (Scion 8300) equipped with a flame ionization detector (FID), manufactured by SCION Instruments. Separation was performed with a capillary column (10.0 m × 530 μm), using hydrogen as the carrier gas. The detector temperature was set to 390 °C. The oven temperature began at 60 °C with a 2 minutes hold, then ramped to 200 °C at a rate of 10 °C min^{-1} (no hold), followed by a ramp to 240 °C at 5 °C min^{-1} with a 7 minutes hold, and finally increased to 390 °C at 12.5 °C min^{-1} with a 20 minutes hold.

2.3. Estimation of WCO molar mass

The WCO was initially transesterified to methyl esters under selected conditions to maximize FAME yield by conventional catalytic transesterification. The reaction was carried out at 65 °C for 3 hours under continuous stirring, using 100 g WCO, 50 g methanol, and 2 g NaOH (97%, Merck). The biodiesel was later separated by funnel separation after the reaction and after each washing with deionized water. The remaining traces of water were evaporated by heating the biodiesel to 110 °C for 3 hours. The peak areas of the resulting FAME components were then analyzed to determine the carbon chain distribution corresponding to the original triglyceride (TAG) branches prior to transesterification. Based on this distribution, the average molar mass of a single TAG branch was calculated according to eqn (1) and then used to estimate the overall molar mass of the triglyceride based on eqn (2).

$$\overline{M}_{\text{branch}} = \sum_i x_i \cdot M_i \tag{1}$$

here, $\bar{M}_{\text{branch}}$ represents the average molar mass of a TAG branch, where x_i refers to the peak area fraction of FAME component i, and M_i is the molar mass of the corresponding fatty acid.

$$\bar{M}_{\text{TGA}} = 3\bar{M}_{\text{branch}} + M_{\text{gl}} - 3(2M_{\text{Hydrogen}} + M_{\text{Oxygen}}) \tag{2}$$

$\bar{M}_{\text{TAG}}$ is the average molar mass of a TAG, while M_{gl}, M_{Hydrogen} and M_{Oxygen} are the molar masses of glycerol and oxygen, respectively.

2.4. Supercritical biodiesel production

The experiments were conducted in a 500 mL SS 316 alloy autoclave (Amar Equipment), capable of operating at temperatures up to 500 °C and pressures up to 350 bar. The reactor was equipped with a hollow-stem stirrer to ensure optimal vertical circulation, and the stirring rate was maintained at 850 rpm. Temperature was measured with a type K thermocouple and pressure was monitored using a piezoresistive sensor mounted on the reactor lid. For each experimental run, the reactor was charged with methanol and WCO, sealed and placed in a heating unit on the testing rig. It was then heated to the desired temperature under continuous stirring. Once the target temperature was reached, nitrogen gas was introduced to achieve the desired pressure. The start time for the reaction was set at the point at which both desired temperature and pressure were reached. At the end of the reaction, heating and stirring were stopped, and active cooling was immediately applied to rapidly reduce the temperature to below 40 °C. The reactor contents were then transferred into a separating funnel and left to settle for one hour, allowing the polar and non-polar phases to separate. The phases were weighed, and samples were filtered using 20 μm syringe filters before being analyzed by GC-FID.

The quality of the product samples was evaluated by analyzing FAME peaks from C14 : 0 to C24 : 1, identified using the same FAME standard solution as previously applied, in accordance with standard EN14103. Quantification of the FAME components were performed using GC-FID with an internal standard method. The response factor between the internal standard and the reference component (C18 : 0) was first determined (eqn (3)). C18 : 0 was selected as a representative component for the total FAME analyte due to its clear chromatographic separation from other FAME peaks and because C18-type components were predominant in the samples. This factor was then used to calculate the FAME (C14 : 0–24 : 1) content in the analyte (eqn (4)), leading to the concentration of FAME in the analyte (eqn (5)). Finally, the biodiesel yield was calculated based on the FAME content relative to the initial feed oil mass (eqn (6)).

$$\mathrm{RF} = \frac{A_{\mathrm{C18:0,st}} \cdot m_{\mathrm{IS}}}{A_{\mathrm{IS}} \cdot m_{\mathrm{FAME,tot,st}} \cdot X_{\mathrm{C18:0,st}}} \quad (3)$$

In this equation, RF is the response factor between the internal standard and the C18 : 0 component, $A_{\mathrm{C18:0,st}}$ is the peak area of C18 : 0, A_{IS} is the peak area of the internal standard, m_{IS} is the mass of the internal standard added to the sample, $m_{\mathrm{FAME,tot,st}}$ is the mass of the total FAME standard analyte and $X_{\mathrm{C18:0,st}}$ is the mass fraction of C18 : 0 in the FAME standard.

$$m_{\mathrm{FAME}} = \left(\frac{A_{\mathrm{FAME}} - A_{\mathrm{IS}}}{A_{\mathrm{IS}}}\right)\left(\frac{m_{\mathrm{IS}}}{\mathrm{RF}}\right) \quad (4)$$

here, m_{FAME} and A_{FAME} represent the mass and peak area of the analyte, covering specifically components from C14 : 0 to 24 : 1, respectively.

$$C_{\mathrm{FAME}} = \frac{m_{\mathrm{FAME}}}{m_{\mathrm{tot}}} \quad (5)$$

C_{FAME} is the concentration of FAME in the analyte and m_{tot} is the total mass of the analyte.

$$Y_{\mathrm{FAME}} = \frac{C_{\mathrm{FAME}} \cdot m_{\mathrm{product}}}{m_{\mathrm{feed}}} \times 100\% \quad (6)$$

Y_{FAME} is the FAME yield of the product sample, m_{product} is the mass of the liquid product after the experimental run, and m_{feed} is the mass of the feed oil.

2.5. Experimental modeling and optimization

The testing matrix for the optimization study was generated using the design of experiments software Design-Expert 13 (Stat-Ease, Inc., Minneapolis, MN, USA), employing a central composite design with a quadratic model to assess system performance. This approach was chosen to enable a comprehensive analysis of both main effects and interactions between factors. Additional extreme points were included to evaluate the robustness of the process and to ensure that the model captured behavior across the full operational range, including potential nonlinear behavior at the boundaries. The design included four factors at three levels, and all experimental runs were randomized to ensure statistical reliability. The full range of the operating conditions are given in Table 1. Biodiesel yield was used as a response variable to evaluate the effect of the experimental conditions. The optimization was performed using the numerical optimization method in Design-Expert. In this approach, goals were set for each factor and the response variable. The goals for the independent variables were set to minimize while the goal for biodiesel yield, the response variable, was set to maximize. A lower limit of 95 wt% biodiesel yield was specified in the optimization to ensure that the yield remained above a defined threshold. This method was used to identify the optimal operating conditions that would maximize biodiesel yield within the defined operational ranges.

Table 1 Process variables and their corresponding ranges used in the experiments

Variable	Code	Range	Unit
Temperature	*A*	200–400	°C
Pressure	*B*	100–200	barg
Methanol : oil (M : O) ratio	*C*	20–40	mol mol^{-1}
Time	*D*	0–60	min

Four validation tests were performed using the optimized parameter levels to confirm the biodiesel yield target within a 95% confidence interval. The resulting biodiesel yield was applied to the statistical analysis in the software to generate a validation table containing prediction accuracy and model performance metrics.

2.6. WCO and biodiesel physical properties

Further analysis of the product samples from the validation tests were performed to obtain properties that are common for evaluating biodiesel quality. However, the samples were first combined into a single composite sample, as they had been produced under identical conditions. Subsequently, methanol was evaporated by heating at 60 °C for four hours, after which the remaining biodiesel was extracted by centrifugation using an ELMI CM-6MT benchtop centrifuge at 2300×*g* for 10 min. Density was measured using an Eraspec Fourier transform infrared spectrometer analyzer (Eralytics), complying fully with ASTM D4052. The measurement of kinematic viscosity was conducted using a Cannon–Fenske viscometer tube (Merck) in accordance with ASTM D445. The total acid number (TAN) was measured according to EN 14104 using KOH (≥85%, Merck) as titrant, to determine fatty acid content.

2.7. Techno-economic analysis

To assess economic viability, a continuous biodiesel production process was developed and simulated in Aspen Plus to convert WCO into FAME using the SCM process, under optimal operating conditions obtained in the experimental part of this study. For the base case scenario, a plant size 10.6 KTA was selected for the process design and simulation. All process modeling, mass and energy balances and separation sequence simulations were performed using Aspen Plus V12.0 using appropriate thermodynamic package (RK for high-pressure systems and UNIQUAC for low-pressure systems) that captures high pressure phase

equilibria and polar–nonpolar interactions, and capital costs were estimated using the Aspen Process Economic Analyzer V12. WCO was represented by three model components: triolein and tripalmitin, which stand in for the unsaturated and saturated triglyceride fractions, respectively, while oleic acid represents the FFA content. In order to size reactor and simulate its performance, appropriate kinetic data were required. The kinetic data for both esterification of FFA and transesterification of triglycerides in SCM were obtained from literature.[21,25] Additionally, its important to note that reactor design under high-pressure and high-temperature conditions is inherently captured within the Aspen Process Economic Analyzer framework, where equipment sizing, wall thickness, and material selection are incorporated into cost estimation, providing a first-order approximation consistent with a Class IV/V estimate. A detailed treatment of mechanical design, materials integrity, and process safety considerations is beyond the scope of this work and would require a dedicated engineering design study.

To estimate the return on investment, a discounted cash flow spreadsheet was developed to estimate the capital expenditure (CAPEX), yearly operating expenditure (OPEX), and revenue over the project lifetime. The total CAPEX was estimated using Aspen Process Economic Analyzer (APEA), where bare equipment costs were calculated based on process simulation outputs, including equipment sizing, construction materials, and operating conditions.

Subsequently, direct and indirect costs were estimated by applying standard cost factors to the bare equipment cost. These factors account for piping, instrumentation and control, electrical systems, civil works, structures, insulation and painting, as well as offsite facilities, engineering, contingency, and working capital. A detailed breakdown of these cost factors is provided in Table S1 of SI.

It was assumed that CAPEX allocation and construction of the plant was completed in the first four years, with plant operation beginning in the fifth year. A standard nominal discount rate of 10.7%, and a total effective income tax rate of 30% were assumed. A methanol price of 340 $ per t, WCO price of 820 $ per t, pharmaceutical grade glycerol price of 1300 $ per t, raw water price of 1.5 $ per m^3, electricity price of 0.07 $ per kWh and natural gas price of 5.5 $ per GJ was assumed in base case scenario. Further details of the financial parameters and raw material costs along with references used in the analysis are listed in Table S2.

A key discussion point here is the cost of WCO used for the analysis. Table 2 summarizes the different prices for WCO pricing in the United States. Many previous TEA studies on biodiesel production *via* the SCM process have assumed very low feedstock costs for WCO, typically in the range of 144–200 $ per t. These values are often derived from restaurant-level rebate figures, but they exclude the costs of transport, aggregation, and pre-treatment/clean-up, and therefore underestimate the true delivered price for biodiesel-grade WCO. On the other hand, internationally traded WCO destined for biodiesel and SAF markets is priced around 1000–1300 $ per t, reflecting higher quality specifications which are not required SCM process which is more accommodating for the feedstock. The most relevant benchmark for our study is U.S. yellow grease, the standard commodity grade of WCO defined by the American Fats & Oils Association, which is already aggregated, dried, and filtered for fuel use. Recent data place yellow grease in the range of 750–900 $ per t, so we adopt 820 $ per t as a base-case feedstock cost for WCO.

2.8. Life cycle carbon footprint analysis

Following the ISO 14040/44 framework, a cradle to gate carbon footprint analysis was conducted to quantify GHG emissions associated with biodiesel production WCO *via* the SCM process. The functional unit was defined as 1 kg of biodiesel. The system boundary encompassed feedstock collection and transport, onsite methanol production, SCM process for biodiesel production and biodiesel use/combustion. The use/combustion phase was included in the system boundary for biodiesel to ensure comparability with conventional diesel. For biodiesel, CO_2 released upon combustion was considered biogenic and therefore assigned a global warming potential (GWP) of zero, in line with IPCC and ISO 14067 guidelines. Other tailpipe emissions such as SO_x and NO_x from biodiesel are typically very low and contribute negligibly to the climate change category. For

Table 2 Comparison of WCO prices in USA

Type	Price range	What it represents	Notes	Ref.
Restaurant/local collection	100–200 $ per t	Rebates restaurants are paid by haulers to remove raw used oil	Excludes collection logistics, transport, pretreatment/cleanup. Oil still contains water, solids, FFA, soaps	26 and 27
U.S. yellow grease	750–904 $ per t	Standard U.S. commodity grade WCO. It is aggregated, dried, filtered, and blended by renderers/collectors	Includes collection + basic cleanup → "biodiesel-ready" feedstock	28 and 29
Commodity/biodiesel- and SAF-grade WCO	1000–1300 $ per t	International biofuel-grade WCO traded for biodiesel and SAF markets	Includes full aggregation, pretreatment, certification, and transport. Premium reflects global SAF/biodiesel demand	30 and 31

conventional diesel, benchmark life-cycle CO_2 emissions (~4 $kgCO_{2eq}$ per kg-diesel[32]) were taken from literature values, which account for both upstream and combustion phases.

Two different scenarios of methanol production: conventional methanol synthesis from natural gas (NG-to-MeOH) and renewable methanol synthesis *via* CO_2 hydrogenation (CO_2-to-MeOH) were assessed. Emissions were quantified based on biodiesel plant operation while impacts associated with construction and infrastructure were not considered. Economic allocation was applied to distribute environmental burdens between biodiesel and the glycerol coproduct. The life cycle inventory analysis was developed primarily on the basis of energy inputs including electricity, steam, and natural gas consumption, as these represent the dominant contributors to GHG emissions for biodiesel production. Material and catalyst inputs were excluded from the system boundary, as their overall contribution to environmental impacts is expected and widely reported to be negligible relative to energy use. The inventory analysis for NG-to-MeOH and CO_2-to-MeOH process units were based on flowsheets reported by Vaswani[33] and Sollai *et al.*[34] and for the DAC unit was based on the study by Casaban *et al.*[35] Data related to WCO collection and transportation were based on 100 km average transportation distance. Upstream emissions related to natural gas extraction and transport were based on reported assessments for North America at ~15 gCO_{2eq} per MJ-NG.[36] Upstream emissions related to grid electricity were based on average grid carbon intensity of USA at ~367 gCO_{2eq} per kWh[37] and for renewable electricity at ~46 gCO_{2eq} per kWh[38] based on numbers for solar photovoltaic plants.

3. Results and discussion

3.1. Experimental biodiesel yields

Experiments were conducted according to the randomized central composite design, following similar statical optimization approaches previously reported in the supercritical biodiesel literature.[39] The resulting biodiesel yields were calculated for each run using the internal standard quantification method described by eqn (3)–(6). These yields were used as the response variable for developing the reduced quadratic model used in this work. Yields ranged from 57.22 wt% to 99.20 wt%, indicating that biodiesel yield was highly influenced by operating conditions. These results provided a solid basis for model fitting and further optimization.

3.2. Model evaluation and diagnostics

The statistical significance of the quadratic response surface model was evaluated using analysis of variance (ANOVA), with the results presented in Table S3. The ANOVA indicates the model is highly significant (F-value = 11.19, p-value < 0.0001), suggesting the quadratic model to effectively represent the relationship with biodiesel yield.

Among linear terms, temperature (A) and the M : O ratio (D) significantly affected yield while pressure (B) and time (C) did not. Significant interactions were AC (temperature–time) and BD (pressure–M : O) with AC the strongest, while AD and CD were not significant. A^2 and D^2 quadratic terms were significant, with A^2 especially strong (F-value = 37.71). The lack-of-fit test is not significant compared to the pure error (F-value = 0.3136, p-value = 0.9277). This confirms the quadratic model adequately fits the experimental data and accurately captures the underlying process trends (Table S4).

The final regression equation for biodiesel yield in terms of coded factors is presented in (eqn (7)). This equation quantifies the factor effects and interactions that the ANOVA identified as significant. The main factors positively influenced yield, with D showing the strongest linear effect (+6.65). Significant interactions included antagonistic effects from AC (−6.50) and BD (−2.99), and a synergistic effect from CD (+1.33). Significant negative quadratic terms for A ($-6.67A^2$) and D ($-2.48D^2$) indicated response curvature and the existence of optimal levels, particularly for temperature (A). This equation provides a basis for predicting and optimizing biodiesel yield within the operating ranges studied.

$$\begin{aligned}\text{Biodiesel yield} = {} & 87.75 + 2.61A + 1.60B + 1.47C \\ & + 6.65D - 6.50AC - 1.10AD - 2.99BD \\ & + 1.33CD - 6.67A^2 - 2.48D^2 \end{aligned} \quad (7)$$

The prediction accuracy of the response surface model was evaluated by plotting predicted biodiesel yields against corresponding experimental values, as presented in Fig. S1a. The data points show a reasonable alignment with the regressed diagonal line, indicating a clear correlation and supporting the model's capability to predict biodiesel yield within the tested parametric ranges. Minor deviations observed around the line result from residual variability, but do not suggest any significant lack of fit, supporting the model's robustness. Moreover, to further assess model adequacy and verify the independence of residuals, externally studentized residuals were plotted against the run order (Fig. S1b). The residuals are randomly distributed around the zero baseline and remain within the statistical control limits of ±3.77, showing no clear patterns or outliers. This random scatter confirms that residuals are independent and that no systematic or time-related factors influenced the experimental results.

3.3. Effects of operating conditions

The effect of process variables on biodiesel yield was derived from the response surface model (Fig. 1). As shown in Fig. 2a and b, reaction temperature displays a strong positive influence on yield, particularly in the range of 250 °C to approximately 330 °C. This effect becomes more noticeable at higher M : O ratio and longer reaction times, indicating significant interaction effects between temperature and these parameters.

The M : O ratio also plays a critical role in enhancing yield. The molar M : O ratio for each experimental run was determined based on the average WCO molar mass estimated using eqn (1) and (2). As shown in Fig. 1b–d, yield increases significantly as the M : O ratio rises from 20 to around 40, after which the effect begins to level off. Reaction time has a similar positive impact, with optimal yields typically observed at durations of 30–45 minutes (Fig. 1d). Both M : O ratio and reaction time

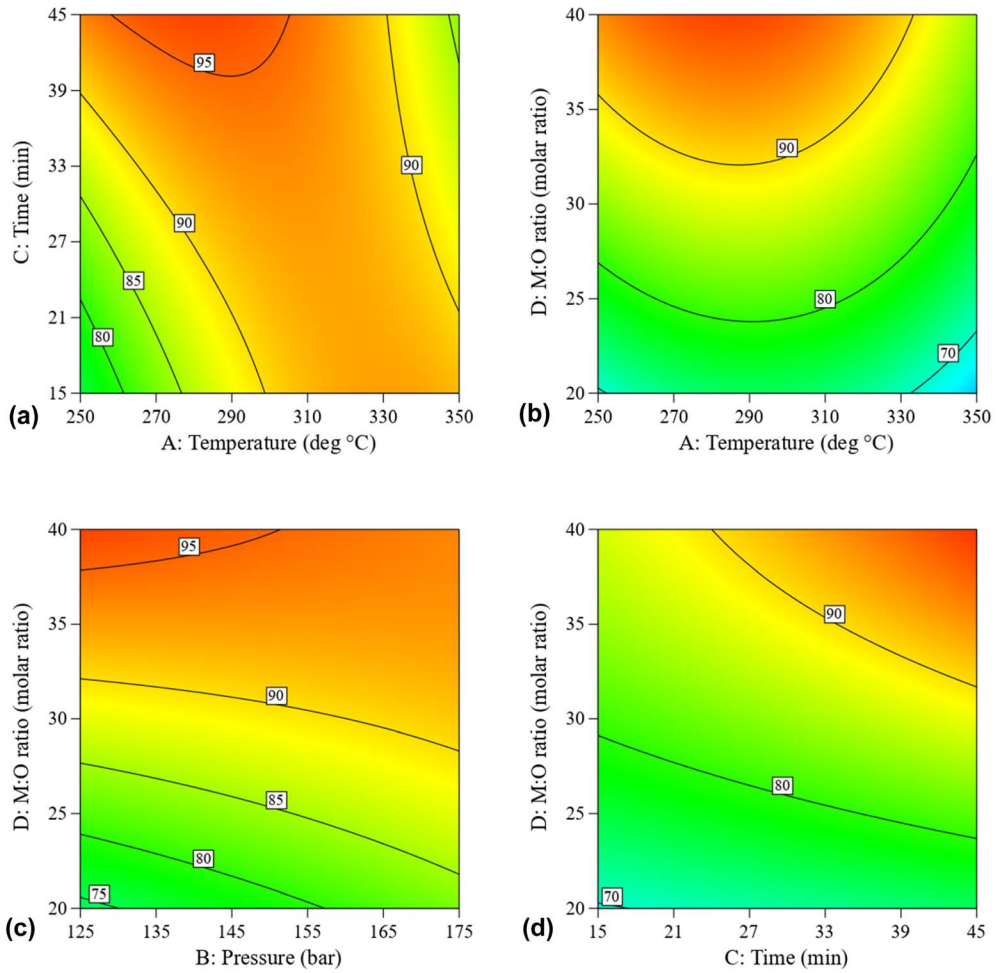

Fig. 1 Contour plots showing effects of process variables on biodiesel yield: (a) time and temperature, (b) M : O ratio and temperature, (c) M : O ratio and pressure, and (d) M : O ratio and time.

show combined effects with temperature and with each other, as high yields are achieved only when all three parameters are sufficiently elevated (Fig. 1d). In contrast, pressure had a relatively limited effect within the tested range of 125–175 bar. When other parameters were held constant at specific levels, a slight negative trend was observed, suggesting that lower pressures may be slightly more favorable (Fig. 1c).

3.4. Optimization of operating conditions

Following the identification of optimal operating conditions through numerical optimization, the predictive accuracy of the response surface model was experimentally validated. Four confirmation runs were carried out using the optimized parameters: 282.8 °C, 125 bar, a M : O ratio of 39.17, and a reaction time of 43.3 min. The yields produced from these experiments are presented in Table 3.

The model predicted a biodiesel yield of 95.92% under these conditions. The validation experiments produced an average yield of 92.28%, calculated using eqn (6), as shown in Table S5. This result closely aligns with the predicted value, corresponding to a relative error of approximately 3.8%. Additionally, the experimental average falls within the 95% prediction interval, confirming the model's reliability and accuracy for predicting biodiesel yield under supercritical conditions within the studied parameter range.

3.5. Physical properties of WCO and supercritical biodiesel

The product obtained from the validation runs exhibited a slightly lighter color compared to the original WCO, as shown in Fig. S2. Further characterization confirmed changes in density and kinematic viscosity following the supercritical transesterification process. The density decreased slightly compared to the initial WCO (0.92 to 0.89 kg m^{-3}). More significantly, the kinematic viscosity was substantially reduced (47.84 to 6.77 cSt). These results confirm the supercritical process effectively produces a product with properties closer to standard biodiesel.

3.6. Process design and techno-economic analysis

Fig. 2 shows the process flow diagram (PFD) where the WCO and methanol in a molar ratio of ~39 : 1 is introduced into a high-pressure reactor operated above methanol's critical point

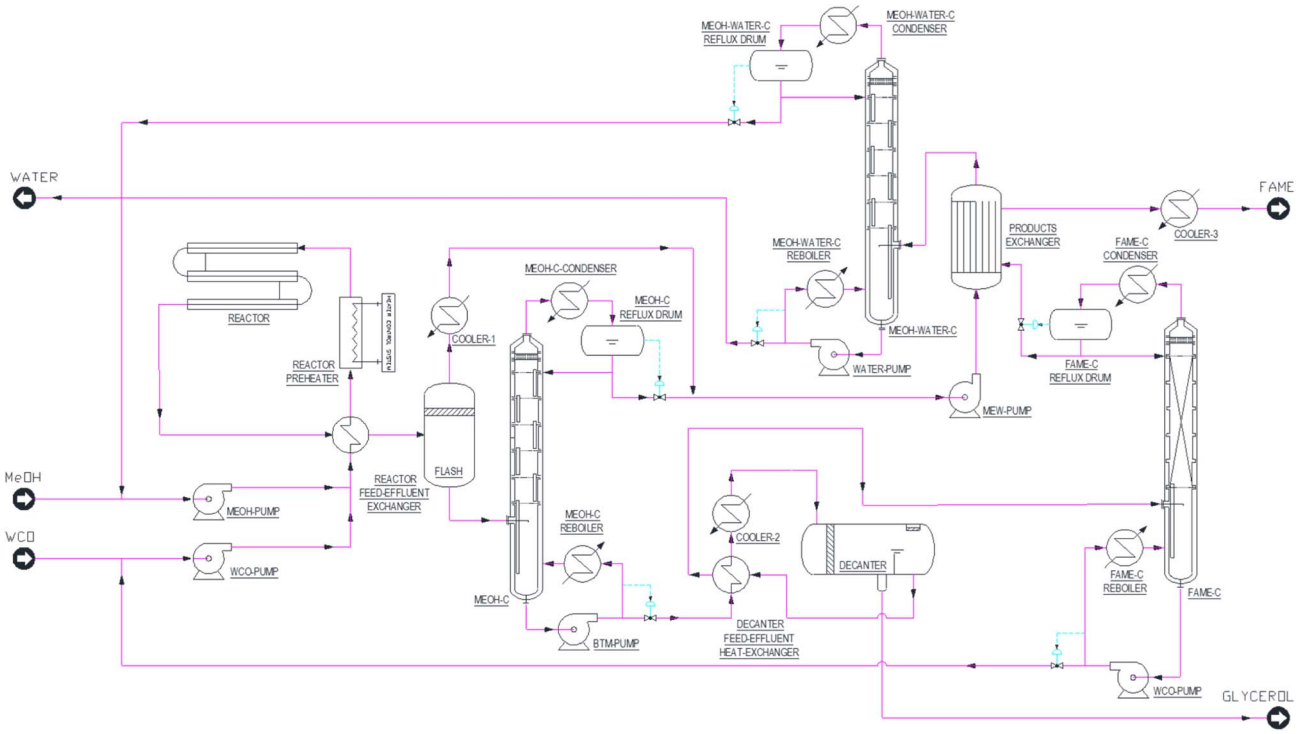

Fig. 2 Process flow diagram of biodiesel production *via* the SCM process.

Table 3 Experimental validation of optimized conditions for biodiesel production

Run	Temperature (°C)	Pressure (barg)	Time (min)	M : O (mol mol^{-1})	Yield (wt%)
V1	282.8	125	43.3	39.17	96.10
V2	282.8	125	43.3	39.17	90.06
V3	282.8	125	43.3	39.17	91.03
V4	282.8	125	43.3	39.17	91.92

(239 °C and 8.1 MPa). A detailed PFD with stream numbers is presented in Fig. S3, with corresponding mass and energy balances in Table S6. At a temperature of 280 °C and pressure of 125 bars, due to the unique physiochemical environment the esterification of FFA's and transesterification of triglycerides proceeds simultaneously. The reactor effluent contains FAME, glycerol, water, and trace unconverted WCO.

The hot reactor effluent is first expanded in a flash drum. Light components, principally methanol and water, exit as vapor and are routed to the water separation column for drying and recycling. The flash liquid, containing FAME, glycerol, and dissolved methanol, proceeds to the first distillation step. In the first distillation column, the bulk of dissolved methanol is separated overhead. This methanol-rich distillate is combined with the flash overhead and sent to the water separation unit. The column bottoms, containing mainly FAME and glycerol with residual methanol, flow to the decanter.

In the decanter, methanol concentration is sufficiently low to allow liquid–liquid separation. The heavy phase is crude glycerol, which can be further refined, and the light phase is a biodiesel-rich stream containing FAME, residual methanol, and trace contaminants. The FAME-rich stream is distilled under vacuum to prevent thermal degradation. The distillate is purified biodiesel product, while the bottoms that contain unconverted WCO are recycled back.

All methanol-rich overheads (from the flash drum, first methanol recovery column, and FAME distillation column) are combined and processed in a water separation unit. This column removes water generated in the process and delivers dry, anhydrous methanol for recycling. Low- and high-pressure steam provide reboiler duty in the distillation columns, while cooling water serves condensers and exchangers. High- and low-pressure steam for column reboilers and other heating duties were generated on-site as part of the OSBL using natural gas as fuel for the steam boilers. The efficiency of the steam boiler was specified at 90% and isentropic efficiency of pumps was taken at 75%.

The raw material (kg per kg-biodiesel) and energy demand (kWh per kg-biodiesel) for the process is presented in Fig. 3. The detailed mass and energy balances are presented in Table S6.

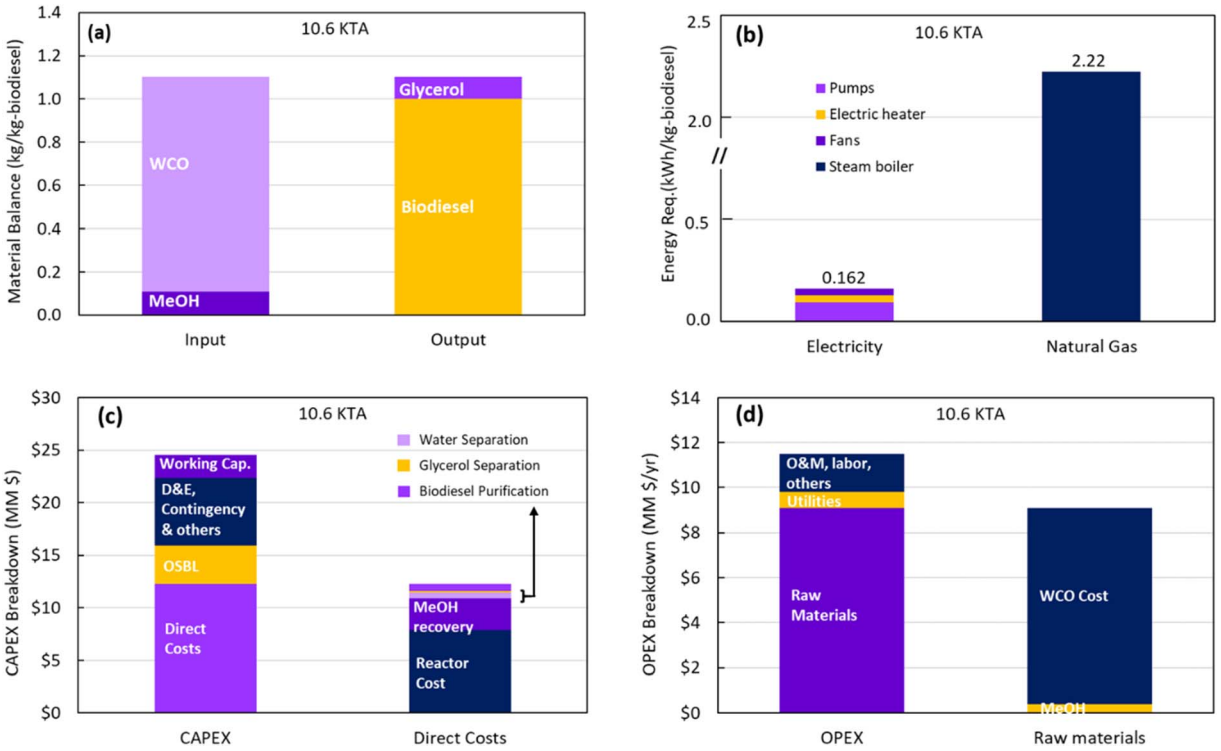

Fig. 3 (a) Raw material (kg kg^{-1}-biodiesel), (b) energy demand (kWh kg-biodiesel), (c) CAPEX (MM$), and (d) OPEX (MM$ per year) for the SCM process for biodiesel production.

For every kg of biodiesel produced, the process consumes approximately 0.99 kg of WCO, 0.11 kg of methanol, along with the coproduction of 0.1 kg of glycerol. The electricity requirement is 0.16 kWh per kg-biodiesel primarily used for pumps. Since we assume on-site production of steam *via* natural gas steam boilers, there is a significant consumption of natural gas at 2.22 kWh per kg-biodiesel or 8 MJ per kg-biodiesel. This is used to produce high-pressure stream at 42 barg and 255 °C at a rate of ~3 kg per kg-biodiesel. The large steam consumption is primarily driven by the distillation requirements to recover or recycle the excess methanol, unconverted WCO and remove excess water.

Fig. 3c shows a breakdown of the capital expenditure (CAPEX) of the plant. The direct costs or ISBL costs are the major contributor at 50% and cover core process units including reactor system high pressure pumping, and downstream separation units such as flash drums, distillation column, decanters, and others. It also includes installation, piping, instrumentation, civil work, site preparation, *etc.* The high direct costs are driven by the high-pressure reactor and methanol recovery units that are sized to deal with the excess methanol. The OSBL costs (15% of total CAPEX) consist of all supporting facilities and infrastructure required for ISBL such as steam boilers, air system (compressors and dryers), and cooling water systems. Finally, a significant portion (~35%) of total capex is for the design, engineering, contingency and working capital. This distribution demonstrates that while the process equipment dominates the expenditure profile, a significant portion is dedicated to enabling infrastructure and risk-mitigation measures.

The OPEX profile (Fig. 3d) of the SCM biodiesel plant is closely tied to the process material balance. To produce 1 kg of biodiesel, approximately 0.99 kg of WCO is required, compared to only about 0.1 kg of methanol. This ratio directly explains why the raw material cost dominates OPEX at ~80%, with WCO being the largest single contributor, while methanol represents only a small fraction. Within the remaining operating costs, utilities contribute less than 10%, largely due to natural gas consumption for steam generation, which reflects the energy intensity of operating at supercritical conditions. Fixed costs such as labor, maintenance, and overhead make up the balance and are relatively minor compared to feedstock requirements.

The levelized cost of biodiesel (LCBD) production in the base case scenario was calculated to be ~1.36 $ per kg-biodiesel (Fig. 4a). In USA, the average refinery pool price for fossil diesel has been at ~1.9 $ per gallon in the last few years.[40] Refiners typically have been reporting refinery margins or profits ~0.2–0.3 $ per gallon.[41,42] This gives us a reasonable estimate of levelized cost of fossil diesel at ~1.7 $ per gallon or ~0.55 $ per kg-diesel. This is the closest market analogue to LCBD as both reflect the cost/value at the production stage before retail, distribution, and taxes. The significantly higher cost for biodiesel underscores the challenge for biodiesel production under baseline conditions. The LCBD is dominated by OPEX with ~78% contribution while the CAPEX only contributes ~22% to the LCBD. Given that the process simulation was conducted under optimized operational conditions

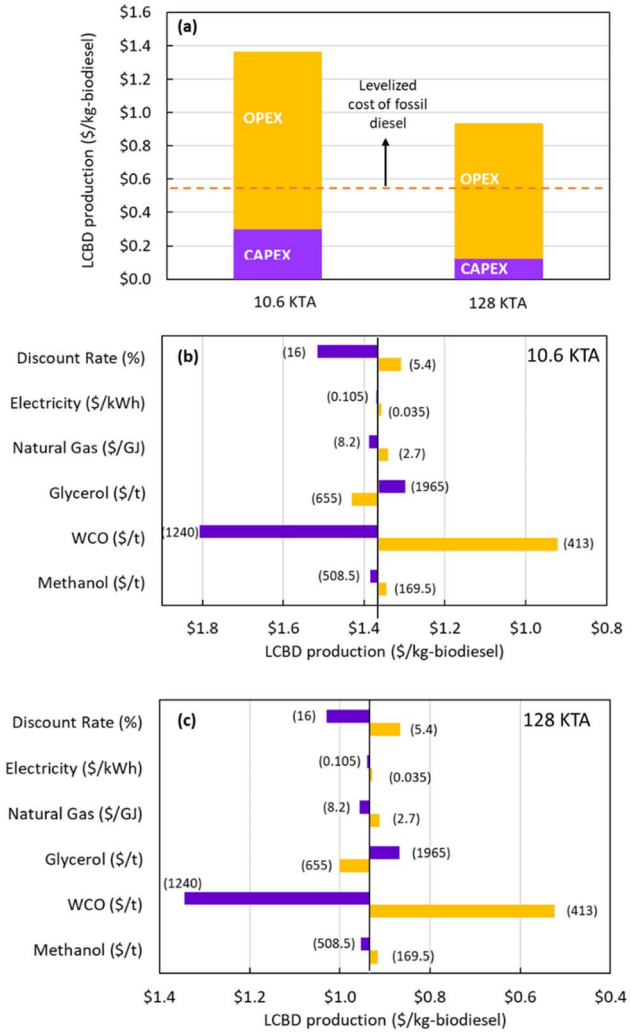

Fig. 4 (a) Levelized cost of biodiesel (LCBD) production ($ per kg-biodiesel) showing capital (CAPEX) and operating (OPEX) cost contributions. Sensitivity analysis of key economic parameters for two plant capacities of: (b) 10.6 KTA and (c) 128 KTA.

to maximize yield, there is limited scope to reduce cost *via* further optimization of process.

To investigate cost-reduction pathways, we first consider economies of scale with a large production capacity of 128 KTA of biodiesel. Employing economies of scale helps reduce CAPEX contribution and reduces the LCBD to approximately 0.94 $ per kg-biodiesel (Fig. 4a), reflecting the expected capital cost dilution and improved fixed cost distribution. While this brings biodiesel closer to parity with fossil diesel, the competitive gap remains when compared against diesel in USA at ~0.55 $ per kg-diesel.[40] We then explored impact of OPEX and economic factors through a sensitivity analysis of the 10.6 KTA plant (Fig. 4b) and 128 KTA plant (Fig. 4c). All parameters except the WCO exhibit only minor impacts on LCBD. The sensitivity analysis revealed that even securing WCO at ~400 $ per t, would not make biodiesel competitive *versus* fossil diesel got the 10.6 KTA plant but will get the LCBD from a larger 128 KTA plant at parity with fossil diesel at ~0.55$ per kg-biodiesel. However, since WCO pricing is outside of any operator's control and subject to market supply and demand effects. Given the limited technical and economic levers available under current market conditions, the final factor to explore competitiveness is the policy environment. Incorporating carbon pricing or low-carbon fuel standards alters the relative economics by increasing the effective cost of fossil diesel. This has been demonstrated for various sustainable technologies. However, this requires a detailed carbon footprint analysis of the SCM process which is discussed next.

3.7. Lifecycle analysis

Fig. 5 shows a block flow diagram depicting the system boundaries in the life cycle carbon footprint study. As described in the methodology section, two alternative pathways for methanol supply were considered: (i) conventional methanol production from natural gas *via* reforming and (ii) renewable methanol from CO_2 hydrogenation, with CO_2 sourced from direct air capture (DAC) and H_2 produced by an alkaline water electrolysis unit. For each pathway, a base-case scenario where grid electricity and natural gas fueled steam boilers are used in the process (1A and 2A) and an optimistic scenario where renewable low-carbon electricity and electric boilers are used (1B and 2B).

Fig. 6a presents the GHG emissions per kilogram of MeOH for each path under different electricity supply scenarios. Emissions are classified into four main contributing factors that are steam production and use, feedstock (H_2/NG/CO_2), electricity use and on-site process related emissions. Under a scenario where grid electricity and steam boilers are used, the CO_2-to-MeOH pathway (2A) leads to very high CI of MeOH at ~5.4 kg-CO_2 per kg-MeOH driven by the high electricity consumption of the water electrolyzer to make H_2 (55 kWh per kg-H_2) and high H_2 consumption of CO_2-to-MeOH process at 0.2 kg-H_2 per kg-MeOH. The second major contributor for both pathways is indirectly from steam use and the natural gas used to generate the steam in the boilers. Although the contribution is similar, the steam requirement is for very different purposes. In the NG-to-MeOH process, steam is used in the NG reformer and for the distillation column (~7.9 MJ-steam per kg-MeOH) while in the CO_2-to-MeOH pathway, steam is used for DAC of CO_2 (~7.8 MJ-steam per kg-MeOH). The use of low-carbon electricity coupled with electric boilers leads to a drastic reduction in CI of methanol from CO_2-to-MeOH pathway (2B) which now has a CI of ~0.8 kgCO_{2eq} per kg-MeOH which is ~20% lower than NG-to-MeOH pathway which has a CI of ~1.02 kg-CO_{2eq} per kg-MeOH (1B). In short, the CO_2-to-MeOH pathway is only viable in case low-carbon renewable electricity is accessible.

Fig. 6b presents the GHG emissions per kilogram of biodiesel based on different scenarios. As mentioned earlier, economic allocation based on a market price of 1.6 $ per kg-biodiesel[43] and 1.3 $ per kg-glycerol[44] was applied to distribute environmental burdens between biodiesel and the glycerol the coproduct. The difference in CI based on the different sources of methanol highlights the importance of this assessment,

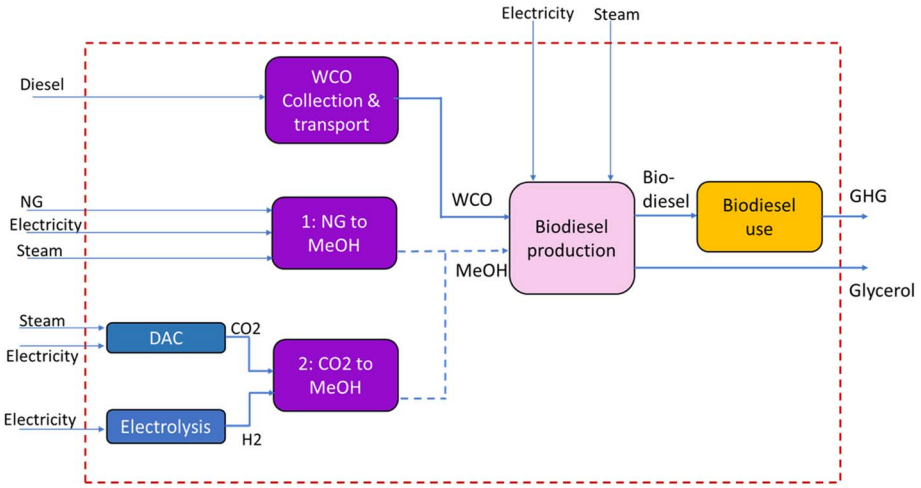

Fig. 5 System boundary and life cycle flow diagram for biodiesel production and use *via* the SCM process with the methanol sourced from two different pathways.

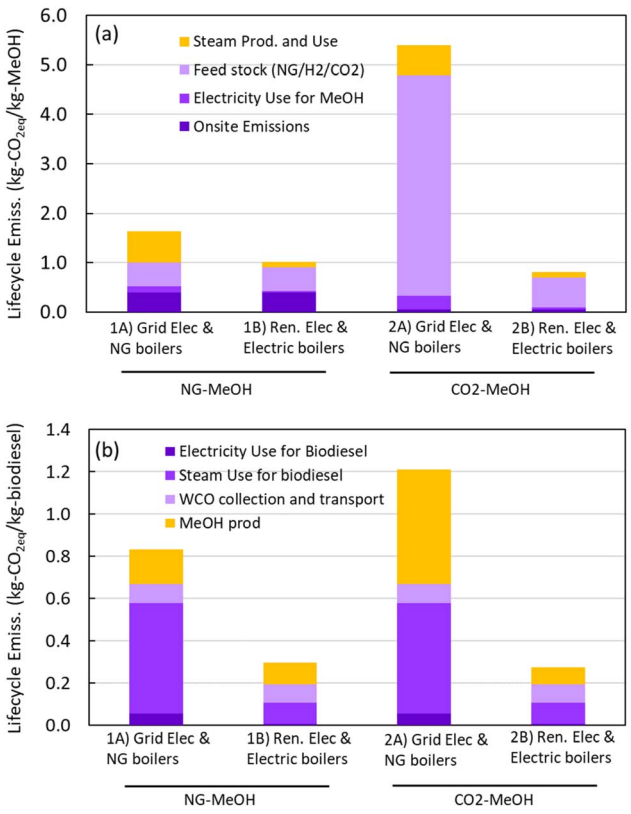

Fig. 6 Life cycle greenhouse gas (GHG) emissions for (a) methanol and (b) biodiesel production under different electricity and heat supply scenarios. Scenarios 1A and 2A represent grid electricity with natural gas boilers, while 1B and 2B represent renewable electricity with electric boilers, for NG-to-MeOH and CO_2-to-MeOH, pathways, respectively.

which has not been reported earlier. Under base case scenario where grid electricity and steam boilers are used, it is better to procure methanol from NG-to-MeOH process (1A) with CI of ~0.83 kg-CO_{2eq} per kg-biodiesel *versus* a CI of ~1.25 kg-CO_{2eq} per kg-biodiesel if methanol is attained from CO_2-to-MeOH process (2A). The steam use in supercritical biodiesel production is significant (3 kg-steam per kg-biodiesel) and is a major contributor to CO_2 emissions in the case of NG-to-MeOH pathway due to use of NG powered steam boilers. However, the emissions from the high use of steam are overshadowed by those related to MeOH production, *i.e.*, H_2 required to make methanol for CO_2-to-MeOH process which leads to the high CI of biodiesel *via* this pathway. Under conditions where on-site electricity and process heat are supplied from renewable sources (including electric boilers), the CI of biodiesel is similar (~0.28–0.30 kgCO_{2eq} per kg-biodiesel) for both methanol supply pathways (1B and 2B). This convergence reflects the dominance of low-carbon energy across biodiesel unit operations, which attenuates the relative contribution of the methanol pathway to total impacts. However, the CO_2-to-methanol route presents broader sustainability advantages—most notably its circular-carbon design (utilizing CO_2 from DAC) and intrinsic compatibility with deep decarbonization trajectories powered by renewable electricity. Lastly, it is important to note that irrespective of the pathway the cradle to grave emissions for biodiesel are significantly lower than conventional fossil fuel which are ~4 kg-CO_{2eq} per kg-diesel. The difference primarily arises during use or combustion of fuel where the CO_2 released from biodiesel is treated as carbon-neutral, so biodiesel emissions are significantly lower on full life-cycle basis. Table 4 summarizes the key findings from life cycle assessment and techno-economic analysis.

In the carbon footprint of the process, the contributions of methanol use, WCO collection, steam, and electricity are discussed. However, it is also important to consider the impact of wastewater treatment. In the supercritical biodiesel production process, the inclusion of methanol and glycerol recovery units and the absence of homogeneous catalysts result in an aqueous stream that is primarily wastewater, although it still contains residual dissolved organics and requires treatment prior to discharge or reuse. The quantity of wastewater generated is very

Table 4 Summary of LCBD and carbon intensity (CI) under different scenarios presented in this study

Summary of TEA results	Capacity (KTA)		LCBD ($ per kg-biodiesel)	
	10.6		1.36	
	128		0.94	
Summary of carbon footprint analysis results	Pathways	Electricity source	Boiler type	CI (kg-CO_{2eq} per kg-biodiesel)
	NG–MeOH	Grid	NG boiler	0.83
	NG–MeOH	Renewable	Electrified boiler	0.30
	CO_2–MeOH	Grid	NG boiler	1.21
	CO_2–MeOH	Renewable	Electrified boiler	0.27

small (~1.93×10^{-6} tonne water per kg biodiesel). Emissions from wastewater treatment arise from direct sources (*e.g.*, CH_4 and N_2O formation) and indirect sources related to energy consumption and are typically reported in the range of 0.3–0.8 kg CO_{2eq} per tonne of wastewater.[45,46] Using an average value of 0.5 kg CO_{2eq} per t-water, the associated emissions are ~9.69×10^{-7} kg CO_{2eq} per kg biodiesel. Accordingly, the results presented in Fig. 6 do not explicitly include emissions from the wastewater stream, as their contribution is negligible.

3.8. Impact of policy tools

The impact of life cycle emissions and policy tools can be gauged *via* the calculation of CO_2 abatement costs (Fig. 7) for biodiesel production. For the assessment of CO_2 abatement costs we considered the base case configuration (Scenario 1A) where methanol is produced from natural gas *via* reforming and grid electricity and natural gas fueled steam boilers are utilized. This is the case for which the technoeconomic analysis was presented earlier in Section 3.6. Additionally, we also considered Scenarios 1B under the reasonable assumption that the cost of using electric boilers will not significantly impact the LCBD. Scenario 2 was not assessed since the cost of methanol produced *via* CO_2-to-MeOH pathway is unknown.

The CO_2 abatement costs was calculated using eqn (8), where $C_{biodiesel}$ is equal to 1.36 $ per kg-biodiesel at a production scale of 10.6 KTA and 0.94 $ per kg-biodiesel at 128 KTA, C_{diesel} is 0.55 $ per kg-diesel, E_{diesel} is equal 4 kg-CO_{2eq} per kg-diesel and $E_{biodiesel}$ are equal to 0.83 kg-CO_{2eq} per kg-biodiesel or 0.3 kg-CO_{2eq} per kg-biodiesel.

$$\text{CO}_2 \text{ abatement cost} = \frac{(C_{\text{biodiesel}} - C_{\text{diesel}})}{(E_{\text{diesel}} - E_{\text{biodiesel}})} \quad (8)$$

Under scenario 1A, with a smaller plant (10.6 KTA) the abatement cost is 255 $ per t-CO_2 decreasing to 123 $ per t-CO_2 for the larger plant (128 KTA). This decreases to 218 $ per t-CO_2 and 105 $ per t-CO_2 under scenario 1B, respectively. These CO_2 abatement costs are very high implying that without policy support it will be difficult to drive economic feasibility.

$$\text{Net CO}_2 \text{ abatement cost} = \text{CO}_2 \text{ abatement cost} - \text{carbon price} \quad (9)$$

The results suggest that carbon pricing can exert a significant influence on the economic feasibility of supercritical biodiesel and is represented by the net CO_2 abatement cost calculated using eqn (9). Specifically, under scenario 1A a carbon price of 120 $ per t-CO_2 enables cost parity between biodiesel and diesel for a large 128 KTA facility and under scenario 1B, a carbon price of 100 $ per t-CO_2 enables cost parity. These findings indicate that a combination of moderate carbon pricing and economies of scale achieved through capital dilution and improved thermal integration can shift supercritical biodiesel production from a system highly sensitive to feedstock costs to a more robust and resilient pathway, de-risking investments for early movers.

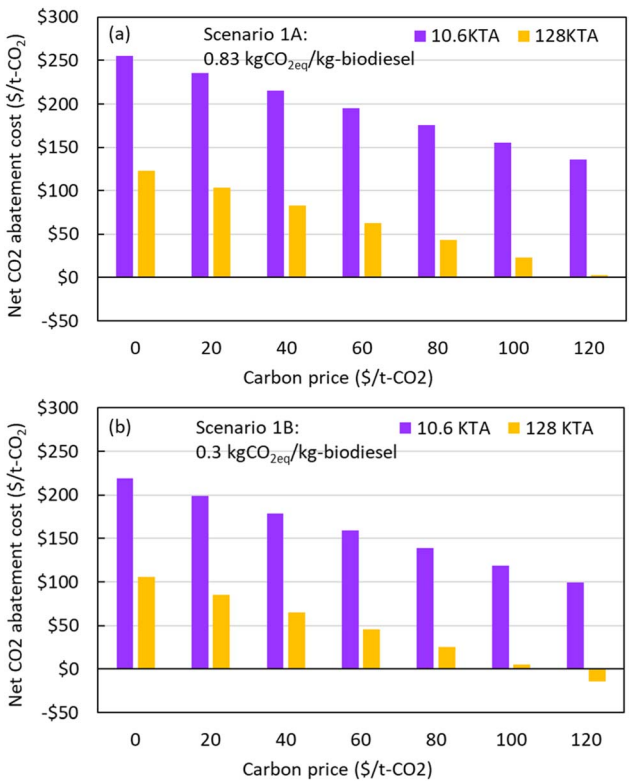

Fig. 7 Net CO_2 abatement costs ($ per t-CO_2) as a function of carbon price for two plant capacities (10.6 and 128 KTA) under (a) Scenario 1A: grid electricity with natural gas boilers and (b) Scenario 1B: renewable electricity with electric boilers.

4. Conclusions

In summary, integrating experimental optimization with process modeling reveals that although biodiesel yields above 92% can be achieved under supercritical conditions, the process remains constrained by its thermal and feedstock

intensity—consuming roughly 1 kg of WCO and 3 kg of steam per kg of biodiesel. TEA showed production costs of 0.9–1.4 $ per kg-biodiesel, underscoring the current gap to fossil diesel competitiveness, while carbon footprint assessment demonstrated that coupling with renewable electricity and modest carbon pricing (~100 $ per t-CO_2) could close this gap for large-scale facilities.

The interplay of these technological, economic, and policy levers ultimately determines the viability and scalability of circular solutions such as WCO to biodiesel within broader decarbonization strategies. Through the analysis presented in this study, we have demonstrated the importance of technology and policy synergies to de-risk large capital investments, catalyze the development of biodiesel supply chains, and enable the accelerated deployment of low-carbon biodiesel as a genuinely sustainable fuel.

Author contributions

Jon Selimi: methodology, validation, formal analysis, investigation, writing – original draft, visualization. Abdullah H. Albin Saad: methodology, software, validation, investigation, writing – original draft. Essra R. Altahir: methodology, software, writing – original draft. Mayasem A. Alsuhami: methodology, software. Mohd Adnan Khan: conceptualization, methodology, formal analysis, writing – original draft, writing – review & editing, supervision. Rashed M. Aleisa: conceptualization, resources, writing – review & editing, supervision. Christian P. Hulteberg: resources, writing – review & editing, supervision. Omar Y. Abdelaziz: conceptualization, methodology, software, resources, writing – review & editing, supervision, project administration, funding acquisition.

Conflicts of interest

The authors declare that they have no known competing financial interest or personal relationships that could have appeared to influence the work reported in this paper.

Data availability

The data that supports the findings of this study are available from the corresponding authors upon reasonable request.

Acknowledgements

The authors acknowledge the financial support provided by Saudi Aramco (Project No. CRAC2339) for the Interdisciplinary Research Center for Refining & Advanced Chemicals at King Fahd University of Petroleum & Minerals (Dhahran, Saudi Arabia).

References

1 A. E. Atabani, A. S. Silitonga, I. A. Badruddin, T. M. I. Mahlia, H. H. Masjuki and S. Mekhilef, A comprehensive review on biodiesel as an alternative energy resource and its characteristics, *Renew. Sustain. Energy Rev.*, 2012, **16**, 2070–2093.

2 A. Demirbas, Biodiesel from waste cooking oil *via* base-catalytic and supercritical methanol transesterification, *Energy Convers. Manag.*, 2009, **50**, 923–927, DOI: 10.1016/j.enconman.2008.12.023.

3 J. Huang, Y. Jian, P. Zhu, O. Abdelaziz and H. Li, Research Progress on the Photo-Driven Catalytic Production of Biodiesel, *Front. Chem.*, 2022, **10**, 1–7, DOI: 10.3389/fchem.2022.904251.

4 G. Knothe, J. Krahl, and J. Van Gerpen, *The Biodiesel Handbook*, Elsevier Inc, 2nd edn, 2010, DOI: 10.1016/C2015-0-02453-4.

5 Y. Umar, O. Velasco, O. Y. Abdelaziz, O. Aboelazayem, M. A. Gadalla, C. P. Hulteberg, *et al.*, A renewable lignin-derived bio-oil for boosting the oxidation stability of biodiesel, *Renew. Energy*, 2022, **182**, 867–878, DOI: 10.1016/j.renene.2021.10.061.

6 A. S. Ramadhas, S. Jayaraj and C. Muraleedharan, Biodiesel production from high FFA rubber seed oil, *Fuel*, 2005, **84**, 335–340.

7 O. Aboelazayem, M. Gadalla and B. Saha, Biodiesel production from waste cooking oil *via* supercritical methanol: Optimisation and reactor simulation, *Renew. Energy*, 2018, **124**, 144–154, DOI: 10.1016/j.renene.2017.06.076.

8 Y. Yu, Q. Ma, M. Xie and M. Zhang, Reaction kinetics and process simulation for biodiesel production from rapeseed oil *via* supercritical transesterification, *Biomass Bioenergy*, 2025, **198**, 1–9.

9 L. C. Mourão, G. B. M. de Souza, I. M. Dias, T. S. S. Ribeiro, J. Pereira, D. C. da Costa, *et al.*, Continuous hydrogen production from biodiesel wastewater treatment *via* supercritical water gasification, *Int. J. Hydrogen Energy*, 2025, **116**, 486–496.

10 S. Saka and D. Kusdiana, Biodiesel fuel from rapeseed oil as prepared in supercritical methanol, *Fuel*, 2001, **80**, 225–231, DOI: 10.1016/S0016-2361(00)00083-1.

11 T. Odisu, A. Akemu, K. O. Obahiagbon and E. C. Anih, Comparative studies on the production of biodiesel from shea nut oil by acid catalyzed and supercritical transesterification processes, *J. Appl. Sci. Environ. Manag.*, 2019, **23**, 349, DOI: 10.4314/jasem.v23i2.23.

12 M. U. Qadeer, M. Ayoub, M. Komiyama, M. U. Khan Daulatzai, A. Mukhtar, S. Saqib, *et al.*, Review of biodiesel synthesis technologies, current trends, yield influencing factors and economical analysis of supercritical process, *J. Clean. Prod.*, 2021, **309**, 127388, DOI: 10.1016/j.jclepro.2021.127388.

13 Y. Nan, J. Liu, R. Lin and L. L. Tavlarides, Production of biodiesel from microalgae oil (Chlorella protothecoides) by non-catalytic transesterification in supercritical methanol and ethanol: Process optimization, *J. Supercrit. Fluids*, 2015, **97**, 174–182, DOI: 10.1016/j.supflu.2014.08.025.

14 S. Karki, N. Sanjel, J. Poudel, J. H. Choi and S. C. Oh, Supercritical Transesterification of Waste Vegetable Oil:

Characteristic Comparison of Ethanol and Methanol as Solvents, *Appl. Sci.*, 2017, **7**, 632, DOI: 10.3390/app7060632.
15 S. A. D'Ippolito, J. C. Yori, M. E. Iturria, C. L. Pieck and C. R. Vera, Analysis of a Two-Step, Noncatalytic, Supercritical Biodiesel Production Process with Heat Recovery, *Energy Fuels*, 2007, **21**, 339–346, DOI: 10.1021/ef060183w.
16 H. He, T. Wang and S. Zhu, Continuous production of biodiesel fuel from vegetable oil using supercritical methanol process, *Fuel*, 2007, **86**, 442–447, DOI: 10.1016/j.fuel.2006.07.035.
17 P. Nagapurkar and J. D. Smith, Techno-economic and life cycle analyses for a supercritical biodiesel production process from waste cooking oil for a plant located in the Midwest United States, *Environ. Dev. Sustain.*, 2023, 1–25, DOI: 10.1007/s10668-023-03064-9.
18 S. Lee, D. Posarac and N. Ellis, Process simulation and economic analysis of biodiesel production processes using fresh and waste vegetable oil and supercritical methanol, *Chem. Eng. Res. Des.*, 2011, **89**, 2626–2642, DOI: 10.1016/j.cherd.2011.05.011.
19 W. Sakdasri, R. Sawangkeaw and S. Ngamprasertsith, Techno-economic analysis of biodiesel production from palm oil with supercritical methanol at a low molar ratio, *Energy*, 2018, **152**, 144–153, DOI: 10.1016/j.energy.2018.03.125.
20 J. M. Marchetti and A. F. Errazu, Technoeconomic study of supercritical biodiesel production plant, *Energy Convers. Manag.*, 2008, **49**, 2160–2164, DOI: 10.1016/j.enconman.2008.02.002.
21 D. Kusdiana and S. Saka, Effects of water on biodiesel fuel production by supercritical methanol treatment, *Bioresour. Technol.*, 2004, **91**, 289–295, DOI: 10.1016/S0960-8524(03)00201-3.
22 C. Kiwjaroun, C. Tubtimdee and P. Piumsomboon, LCA studies comparing biodiesel synthesized by conventional and supercritical methanol methods, *J. Clean. Prod.*, 2009, **17**, 143–153, DOI: 10.1016/j.jclepro.2008.03.011.
23 L. Lombardi, B. Mendecka and E. Carnevale, Comparative life cycle assessment of alternative strategies for energy recovery from used cooking oil, *J. Environ. Manage.*, 2018, **216**, 235–245, DOI: 10.1016/j.jenvman.2017.05.016.
24 S. Morais, T. M. Mata, A. A. Martins, G. A. Pinto and C. A. V. Costa, Simulation and life cycle assessment of process design alternatives for biodiesel production from waste vegetable oils, *J. Clean. Prod.*, 2010, **18**, 1251–1259, DOI: 10.1016/j.jclepro.2010.04.014.
25 O. Aboelazayem, O. Abdelaziz, M. Gadalla, C. Hulteberg, and B. Saha, *Biodiesel Production from High Acid Value Waste Cooking Oil Using Supercritical Methanol: Esterification Kinetics of Free Fatty Acids*, ETA-Florence Renewable Energies, 2017, pp. 1381–1387.
26 Mike, How Much Is Used Oil Worth?, *Grease Connect 2025*, https://greaseconnections.com/used-cooking-oil-prices-in-2025-how-much-is-used-cooking-oil-worth/, accessed on October 1, 2025.
27 A. Kamalov, How Much Is Used Cooking Oil Worth, *Liq Recovery Solut 2024*, https://liquidrecover.com/how-much-is-used-cooking-oil-worth/, accessed on October 1, 2025.
28 Restaurant Technologies, How Much is Used Cooking Oil Worth, *BACK-HOUSE BLOG 2024*, https://www.rti-inc.com/blog/how-much-is-used-cooking-oil-worth/, accessed on October 1, 2025.
29 YELLOW GREASE, Commodity 3, https://www.commodity3.com/instrument/TLW1MNF1/yellow-grease, accessed on October 1, 2025.
30 V. Prykhodko, UCO prices reach two-year high in 2024, increases to continue in 2025 amid demand, *Fastmarkets 2025*, https://www.fastmarkets.com/insights/uco-prices-reach-two-year-high-in-2024-increases-to-continue-in-2025-amid-demand/, accessed on October 1, 2025.
31 J. Morciani, Used cooking oil (UCO) price forecast: a cornerstone feedstock for sustainable aviation fuel, *Fastmarkets 2025*, https://www.fastmarkets.com/insights/used-cooking-oil-forecast-a-cornerstone-feedstock-for-sustainable-aviation-fuel/, accessed on October 1, 2025.
32 British Columbia, *Carbon Intensity Records under the Renewable and Low Carbon Fuel Requirements Regulation*, Ministry of Energy, Mines and Petroleum Resources, Victoria, BC, 2010.
33 S. Vaswani, *Development of Models for Calculating the Life Cycle Inventory of Methanol by Liquid Phase and Conventional Production Processes*, North Carolina State University, 2000.
34 S. Sollai, A. Porcu, V. Tola, F. Ferrara and A. Pettinau, Renewable methanol production from green hydrogen and captured CO2: A techno-economic assessment, *J. CO2 Util.*, 2023, **68**, 102345, DOI: 10.1016/j.jcou.2022.102345.
35 D. Casaban and E. Tsalaporta, Life cycle assessment of a direct air capture and storage plant in Ireland, *Sci. Rep.*, 2023, **13**, 18309, DOI: 10.1038/s41598-023-44709-z.
36 C. L. Weber and C. Clavin, Life Cycle Carbon Footprint of Shale Gas: Review of Evidence and Implications, *Environ. Sci. Technol.*, 2012, **46**, 5688–5695, DOI: 10.1021/es300375n.
37 Frequently Asked Questions (FAQs) - U.S. Energy Information Administration (EIA), https://www.eia.gov/tools/faqs/faq.php?id=74&t=11, accessed on October 3, 2025.
38 National Renewable Energy Laboratory, *Life Cycle Greenhouse Gas Emissions from Electricity Generation: Update*, Golden, CO, 2021.
39 M. A. Shaah, M. S. Hossain, F. Allafi, M. O. Ab Kadir and M. I. Ahmad, Biodiesel production from candlenut oil using a non-catalytic supercritical methanol transesterification process: optimization, kinetics, and thermodynamic studies, *RSC Adv.*, 2022, **12**, 9845–9861, DOI: 10.1039/D2RA00571A.
40 U.S. Total Refiner Petroleum Product Prices, https://www.eia.gov/dnav/pet/pet_pri_refoth_dcu_nus_a.htm, accessed on October 10, 2025.
41 N. Jao, and T. Dhumal, Valero beats estimates as refining margins offset renewable diesel loss, *Reuters*, 2025.

42 Marathon Petroleum Corp., *Reports Second-Quarter 2025 Results*, Marathon Pet Corp, https://ir.marathonpetroleum.com/investor/news-releases/news-details/2025/Marathon-Petroleum-Corp–Reports-Second-Quarter-2025-Results/default.aspx, accessed on October 10, 2025.
43 Biodiesel Sourcing Guide & Market Intelligence, *ProcurementIQ*, https://www.procurementiq.com/market-intelligence/biodiesel, accessed on October 10, 2025.
44 Glycerol Price in United States, *Tridge*, https://dir.tridge.com/prices/glycerol/US, accessed on October 10, 2025.
45 H. Hua, S. Jiang, Z. Yuan, X. Liu, Y. Zhang and Z. Cai, Advancing greenhouse gas emission factors for municipal wastewater treatment plants in China, *Environ. Pollut.*, 2022, **295**, 118648, DOI: 10.1016/j.envpol.2021.118648.
46 Greenhouse gas reporting: conversion factors 2023, *GOVUK 2023*, https://www.gov.uk/government/publications/greenhouse-gas-reporting-conversion-factors-2023, accessed on March 27, 2026.

